Curr Microbiol (2015) 70:27–34
DOI 10.1007/s00284-014-0678-5

PSI Showed Higher Tolerance to Sb(V) than PSII Due to Stimulation of Cyclic Electron Flow Around PSI

Shuzhi Wang · Xiangliang Pan · Daoyong Zhang

Received: 8 June 2014 / Accepted: 1 July 2014 / Published online: 21 August 2014

Abstract The knowledge of the effects of Sb(V) on the physiological characteristics of cyanobacteria was still limited. In the present study, responses of photosystem I and II (PSI and PSII), cyclic electron flow (CEF), and interphotosystem electron transport of *Microcystis aeruginosa* to 5–100 mg/l Sb(V) were synchronously measured using the Dual-PAM-100. 5 mg/l Sb (V) significantly inhibited PSII activity, but had no significant effects on PSI activity. At higher concentrations of Sb(V), the quantum yield and electron transport of PSI were less affected compared to PSII. The ratio of *Y*(II)/*Y*(I) significantly decreased with increasing Sb(V) concentration. It decreased from 0.7 for control to 0.4 for 100 mg/l Sb(V)-treated cells, indicating that the change of the distribution of quantum yields between two photosystems and more serious inhibition of PSII under stress of Sb(V) compared to PSI. CEF was activated associated with the inhibition of linear electron flow after exposure to Sb(V). The contribution of *Y*(CEF) to the quantum yield and activity of PSI increased with increasing Sb(V) concentrations. The cyclic electron transport rate made a significant contribution to electron transport rate of PSI, especially at high Sb(V) concentration (100 mg/l) and high illumination (above 555 μmol photons/m^2/s). The stimulation of CEF was essential for the higher tolerance of PSI than PSII to Sb(V).

S. Wang · X. Pan (✉) · D. Zhang
Laboratory of Environmental Pollution and Bioremediation, Xinjiang Institute of Ecology and Geography, Chinese Academy of Sciences, Urumqi 830011, China
e-mail: xlpan@ms.xjb.ac.cn

S. Wang
Graduate University of Chinese Academy of Sciences, Beijing 100049, China

D. Zhang
State Key Laboratory of Environmental Geochemistry, Institute of Geochemistry, Chinese Academy of Sciences, Guiyang 550002, China

Introduction

Antimony (Sb) is a trace element widely distributed in the lithosphere [26]. Sb is not the essential element required for biological metabolism and is potentially toxic even at low concentrations [28]. Due to its toxicity and ubiquitously present in the environment, Sb is considered as a global contaminant [30]. Sb is widely used in various industries and daily life, including production of optoelectronic devices [3], coloring matter, brake lining, and flame retardant [28]. Sb pollution has become a growing environmental concern since large amount of Sb has been released into the environment during its utilization.

There have sufficient evidence proved that Sb_2O_3 was carcinogenic [12]. But the knowledge about toxicity of Sb to plants and microorganisms was still limited. A few studies suggested that Sb had adverse influences on growth and chlorophyll synthesis of plants [7, 21]. Since Sb is found to be widespread in aquatic environment [19], it has significant meaning to evaluate the toxicity of Sb to aquatic organisms. Antimony is present mainly as Sb(V) in the aqueous extractable fraction [26]. So the effects of Sb(V) on the physiological characteristics of cyanobacteria need to be addressed.

Limited studies showed that both Sb(III) and Sb(V) could inhibit oxygen evolution and photosystem II (PSII) activities of cyanobacteria [33, 35]. However, the effects of Sb on the activities and electron transport of photosystem I (PSI) were still unclear. In most cases, effects of heavy metals on PSII or PSI were studied separately although simultaneous measurements of activities of PSI and PSII after exposure to heavy

metals are necessary, which could provide more accurate information about effects of heavy metals on photosynthetic apparatus [34]. In addition, a few recent studies reported the stimulation of cyclic electron flow (CEF) around PSI under stress and its important role in photoprotection and photosynthesis [9, 10, 34]. Whether Sb exposure could stimulate CEF around PSI and effect of Sb on CEF are unknown.

In the present study, *Microcystis aeruginosa* was used to detect the effects of Sb(V) on PSII and PSI activities. *M. aeruginosa* has often been used as a model microbial species for examining effects of contaminants on photosynthesis [33, 36]. The aim of this work was to detect responses of quantum yields of energy conversion in PSI and PSII and CEF, and the changes of electron transport between two photosystems and CEF at various concentrations of Sb(V) and increasing illumination.

Materials and Methods

Culture of *Microcystis aeruginosa*

Microcystis aeruginosa (FACHB-905) was purchased from Freshwater Algae Culture Collection of Institute of Hydrobiology, Chinese Academy of Sciences (Wuhan, China). The cells were cultured in BG-11 medium [29]. All the cultures were carried out at 25 °C under 30 μmol photons/m^2/s with a 12:12 h light: dark cycle. The growth of cultures was monitored daily by testing optical density at 680 nm (OD_{680}) with a UV2800 spectrophotometer (Unico, Shanghai, China). The cells in exponential growth phase were harvested for further experiments.

Sb(V) Treatments

Sb(V) was applied in the form of analytical-grade potassium pyroantimonate (Aladdin Reagent Database Inc., Shanghai, China). The *M. aeruginosa* cells were cultured in 50-ml flasks with 25 ml of BG-11 medium containing various concentrations (0, 5, 50, and 100 mg/l) of Sb(V). High concentrations of Sb(V) up to 100 mg/l were set for evaluation of its toxicity because Sb in polluted surface water near a Sb mine is 24.02–42.03 mg/l [7]. Each treatment was quadruplicated. The samples with 0 mg/l Sb(V) were used as control. All treatments were run under the same culture condition as described above. Measurements were carried out at 72 h after onset of Sb(V) treatments.

Measurement

Application of the Dual-PAM-100 System

PSII and PSI activities were measured in the mode of cyanobacteria using a dual-wavelength pulse-amplitude-modulated fluorescence monitoring system (Dual-PAM-100, Heinz Walz GmbH, Effeltrich, Germany). The Dual-PAM-100 system can detect $P700^+$ absorbance changes and chlorophyll a fluorescence at the same time [5, 22, 31].

The sample was injected into the DUAL-K25 quartz glass cuvette, which was then sandwiched between the emitter head and detector head of the system. Each sample was dark adapted for 5 min, and then saturation pulse and actinic light were applied according to the measurement routine. Parameters were automatically calculated by the Dual-PAM-100 software during the measurement [22].

Fluorescence and $P700^+$ Signal After Dark Adaptation

$P700^+$ absorbance changes and chlorophyll *a* fluorescence were detected after the cells were dark adapted. Saturation Pulse method was used to detect the maximal change in $P700^+$ signal and the maximum fluorescence [14, 22]. The minimal fluorescence after dark adaptation (F_0) was measured by a light at low intensity. A saturating pulse at an irradiance of 10,000 μmol photons/m^2/s was then applied for 300 ms to detect the maximum fluorescence (F_m). P700 redox state was measured as change in $P700^+$ signal with a dual-wavelength (830/875 nm) unit. The maximal change in $P700^+$ signal (P_m) was determined through application of a saturation pulse after far-red pre-illumination for 10 s according to the methods of Klughammer and Schreiber [14, 16].

Rapid Light Curves (RLCs)

After the determination of F_0, F_m, and P_m, rapid light response curves (RLCs) of quantum yields and electron transport rates were performed with the routine program of the Dual-PAM-100 software. During the RLC mode, the actinic light was applied at each photosynthetic active radiation (PAR, which was measured as the photosynthetic photon flux density) for 30 s with increasing intensities (30, 46, 77, 119, 150, 240, 363, 555, 849, and 1,311 μmol photons/m^2/s) to conduct the rapid light response reaction. After each period of actinic light, a saturating pulse was applied to determine the maximum fluorescence signal (F'_m) and maximum $P700^+$ signal (P'_m) under actinic light. P'_m was defined in analogy to the fluorescence parameter F'_m and determined similarly to P_m but without far-red illumination [10].

The quantum yields of PSI and PSII were detected in the RLC mode and calculated automatically from the fluorescence and $P700^+$ signals using the Dual-PAM software. The quantum yields of energy conversion in PSI were calculated according to Klughammer and Schreiber [16] and Wang et al. [29]:

$$Y(\mathrm{I}) = \left(P'_{\mathrm{m}} - P\right)/P_{\mathrm{m}} \quad (1)$$

$$Y(\mathrm{ND}) = (P - P_0)/P_{\mathrm{m}} \quad (2)$$

$$Y(\mathrm{NA}) = \left(P_{\mathrm{m}} - P'_{\mathrm{m}}\right)/P_{\mathrm{m}}, \quad (3)$$

where Y(I) was effective photochemical quantum yield of PSI, Y(ND) was the quantum yield of non-photochemical energy dissipation in PSI reaction centers due to donor-side limitation, and Y(NA) was the quantum yield of non-photochemical energy dissipation of PSI reaction centers due to acceptor side limitation. P was the $P700^+$ signal recorded just before a saturation pulse. Then, a saturation pulse was applied to determine the maximum $P700^+$ signal under actinic light (P'_{m}). The minimum level of the $P700^+$ signal (P_0) was tested at a 1 s dark interval after each saturation pulse. The signals P and P'_{m} were determined referring to P_0.

The quantum yields of energy conversion in PSII were calculated according to the method of Kramer et al. [16], and transformed into the following simpler equations [15, 31]:

$$Y(\mathrm{II}) = \left(F'_{\mathrm{m}} - F\right)/F'_{\mathrm{m}} \quad (4)$$

$$Y(\mathrm{NPQ}) = F/F'_{\mathrm{m}} - F/F_{\mathrm{m}} \quad (5)$$

$$Y(\mathrm{NO}) = F/F_{\mathrm{m}}, \quad (6)$$

where Y(II) was the effective photochemical quantum yield of PSII, Y(NPQ) was the quantum yield of light-induced non-photochemical fluorescence quenching, and Y(NO) was the quantum yield of non-light-induced non-photochemical fluorescence quenching.

The quantum yield of CEF was calculated from the difference between Y(I) and Y(II) [9]:

$$Y(\mathrm{CEF}) = Y(\mathrm{I}) - Y(\mathrm{II}). \quad (7)$$

The ratios of Y(CEF)/Y(I), Y(II)/Y(I), and Y(CEF)/Y(II) after exposure to various concentrations of Sb(V) were also calculated. These parameters were used to show the change of the distribution of quantum yields between two photosystems and the change of the ratio of quantum yield of CEF to that of linear electron flow (LEF) [4, 9].

Electron transport rates in PSI and PSII, i.e., ETR(I) and ETR(II), were calculated and recorded by the Dual-PAM software [31, 34]. Descriptive parameters of ETR(I) and ETR(II) during the light response reaction were derived from the RLCs. The following parameters were automatically calculated by the Dual-PAM-100 software according to the exponential function [13, 23]: α, the initial slope of RLCs of ETR(I) or ETR(II), reflecting the photon-capturing efficiency [20]; $\mathrm{ETR}_{\mathrm{max}}$, the maximal electron transport rates in PSI or PSII; and I_{k}, the index of light adaptation of PSI or PSII, which was calculated as $\mathrm{ETR}_{\mathrm{max}}/a$.

The cyclic electron transport rate was calculated as ETR(I) − ETR(II) [10], which was used to investigate whether CEF was stimulated and its physiological role under Sb(V) and high light stress.

Statistics

Means and standard error (SE) were calculated for each treatment ($n = 4$). Analysis of Variance (one-way ANOVA) was performed to detect the significance of differences between different treatments. Significant difference was determined by Duncan's multiple range test (DMRT, $P < 0.05$).

Results

Effects of Sb(V) on Quantum Yields of PSI, PSII and CEF

The RLCs of Y(I), Y(II), and Y(CEF) were recorded after the cells were exposed to various concentrations of Sb(V) for 72 h (Fig. 1). Y(I), Y(II), and Y(CEF) decreased with increasing PAR from 30, 46, 77, 119, 150, 240, 363, 555, 849 to 1,311 μmol photons/m^2/s (Fig. 1). Both Y(I) and Y(II) decreased with increasing Sb(V) concentration. The differences of Y(II) were significantly different between different treatments during the entire light response reaction. The difference of Y(II) between different treatments was larger than that of Y(I). Y(CEF) gradually showed differences between different treatments as the PAR intensity increased. Y(CEF) increased with increasing Sb(V) concentration.

Changes of the Ratios of Y(CEF)/Y(I), Y(II)/Y(I) and Y(CEF)/Y(II)

The ratios of Y(CEF)/Y(I) and Y(CEF)/Y(II) increased with increasing Sb(V) concentration. Y(CEF)/Y(II) increased from 0.3 for control to 1.5 for 100 mg/l Sb(V) treatment. On the other hand, Y(II)/Y(I) significantly decreased with increasing Sb(V) concentration. It decreased from 0.7 for the control to 0.4 for the cells treated with 100 mg/l Sb(V) (Fig. 2). When the cells were exposed to 100 mg/l Sb(V), Y(CEF) contributed to most part of Y(I), with an increase of Y(CEF)/Y(I) to 0.6 and a decrease of Y(II)/Y(I) to 0.4.

Quantum Yields of Energy Conversion in PSI and PSII

Quantum yields of energy conversion in two photosystems were recorded after the last procedure of illumination at the highest intensity (1,311 μmol photons/m^2/s) during the

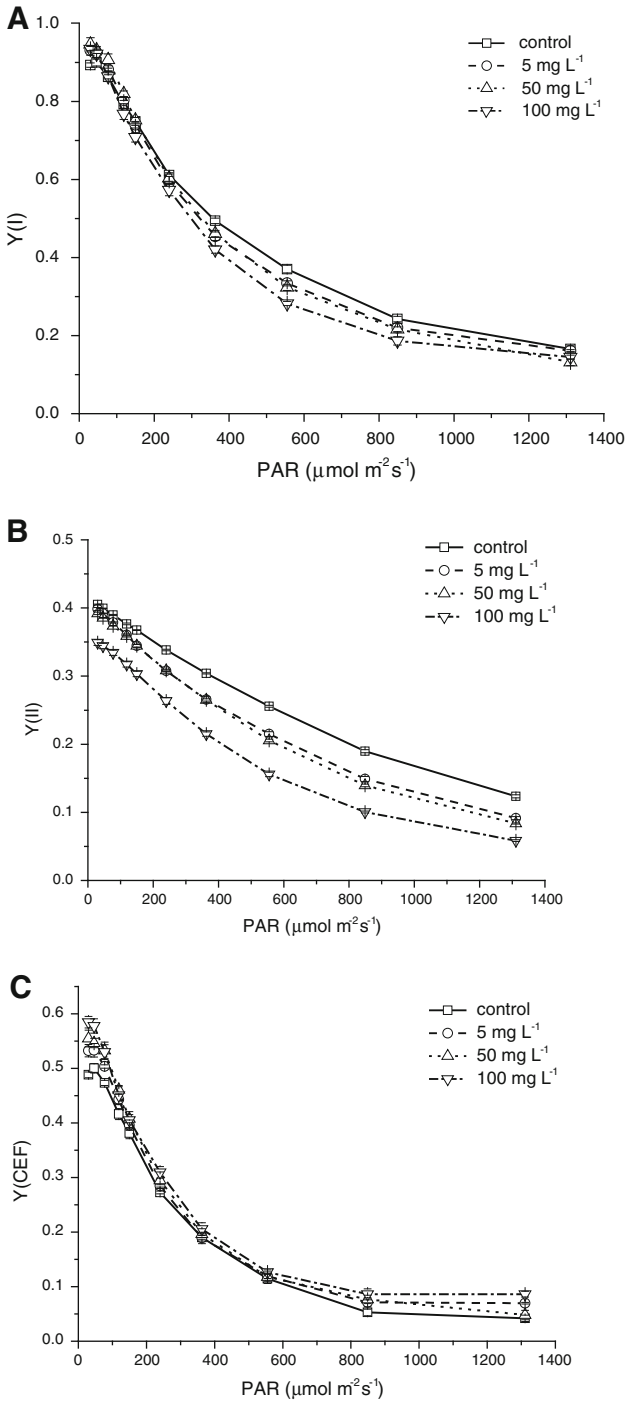

Fig. 1 Quantum yields of the two photosystems and cyclic electron flow (CEF) after exposure to various concentrations of Sb(V) for 72 h. Data were detected during the rapid light response reaction, where PAR was increasing gradually as 30, 46, 77, 119, 150, 240, 363, 555, 849, and 1,311 (μmol/m^2/s). The photochemical quantum yield of **a** PSI, **b** PSII, and **c** CEF. Data were presented as mean ± SE ($n = 4$)

rapid light response reaction (Table 1). *Y*(I) decreased with increasing Sb(V) concentration and were significantly low when the cells were treated with 50 mg/l Sb(V). *Y*(ND) increased with increasing Sb(V) concentration and were

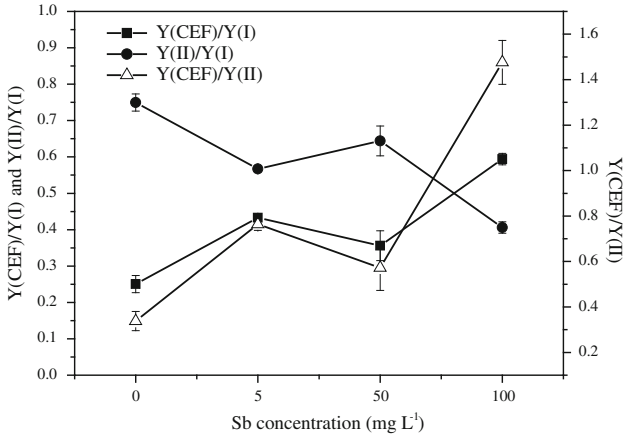

Fig. 2 The changes of the ratios of *Y*(CEF)/*Y*(I), *Y*(II)/*Y*(I), and *Y*(CEF)/*Y*(II) after exposure to various concentrations of Sb(V) for 72 h. *Y*(CEF)/*Y*(I) and *Y*(II)/*Y*(I) indicated the contribution of cyclic electron flow (CEF) and linear electron flow (LEF) to the yield of PSI. *Y*(CEF)/*Y*(II) indicated the ratio of quantum yield of CEF to LEF. Data were recorded after the last procedure of illumination at the highest intensity (1,311 μmol/m^2/s) during the rapid light response reaction. Data were presented as mean ± SE ($n = 4$)

significantly high when the cells were treated with 100 mg/l of Sb(V). Sb(V) treatment had more serious effects on *Y*(II) and *Y*(NO) than on other parameters. *Y*(II) decreased significantly with the increase of Sb(V) concentration, and showed significant differences between each treatment ($P < 0.05$, DMRT). *Y*(NO) increased significantly as the Sb(V) concentration increased, and *Y*(NO) was significantly higher for the cells exposed to Sb(V) compared to control ($P < 0.05$, DMRT). *Y*(NA) and *Y*(NPQ) showed no significant differences between different treatments.

Effects of Sb(V) on RLCs of PSI, PSII and CEF

The RLCs of ETR(I) and ETR(II) dropped with increasing Sb(V) concentration after 72 h of treatment (Fig. 3). The amplitudes of the whole RLCs of ETR(I) were higher than that of ETR(II). RLCs of ETR(I) slightly decreased with increasing concentration of Sb(V) and significantly decreased at 50 and 100 mg/l Sb(V). The RLCs of ETR(II) decreased more than that of ETR(I) due to Sb(V) treatment. ETR(II) of the Sb(V)-treated cells were significantly lower compared to the control.

Descriptive parameters of the RLCs of ETR(I) and ETR(II) showed more information about light response of PSI and PSII under Sb(V) stress (Table 2). I_k, α, and ETR_{max} of the RLCs of ETR(I) did not show significant difference under treatments at ≤5 mg/l Sb(V). I_k and ETR_{max} of the RLCs of ETR(I) decreased with increasing Sb(V) concentration and significantly decreased at 50 and 100 mg/l Sb(V) compared to control ($P < 0.05$, DMRT). α of the RLCs of ETR(I) increased at 50 mg/l Sb(V).

Table 1 The complementary quantum yields of energy conversion in PSI and PSII after exposure to various concentrations of Sb(V) for 72 h

Sb(V) concentration (mg/l)	Quantum yields in PSI			Quantum yields in PSII		
	Y(I)	*Y*(ND)	*Y*(NA)	*Y*(II)	*Y*(NO)	*Y*(NPQ)
0	0.166 ± 0.008[a]	0.828 ± 0.011[b]	0.013 ± 0.009[a]	0.122 ± 0.002[a]	0.825 ± 0.005[c]	0.050 ± 0.003[a]
5	0.161 ± 0.003[a]	0.821 ± 0.013[b]	0.018 ± 0.012[a]	0.092 ± 0.002[b]	0.862 ± 0.006[b]	0.048 ± 0.003[a]
50	0.132 ± 0.009[b]	0.847 ± 0.015[a,b]	0.023 ± 0.010[a]	0.084 ± 0.001[c]	0.875 ± 0.006[a,b]	0.040 ± 0.005[a]
100	0.145 ± 0.005[a, b]	0.875 ± 0.010[a]	0.002 ± 0.002[a]	0.059 ± 0.001[d]	0.894 ± 0.009[a]	0.050 ± 0.084[a]

Data were recorded after the last procedure of illumination at the highest intensity (1,311 μmol photons/m^2/s) during the rapid light response reaction, where PAR was increasing gradually as 30, 46, 77, 119, 150, 240, 363, 555, 849, and 1,311 (μmol photons/m^2/s)

[a, b, c, d] Data were mean ± SE ($n = 4$), and data followed by different letters in the same column are significantly different ($P < 0.05$, DMRT)

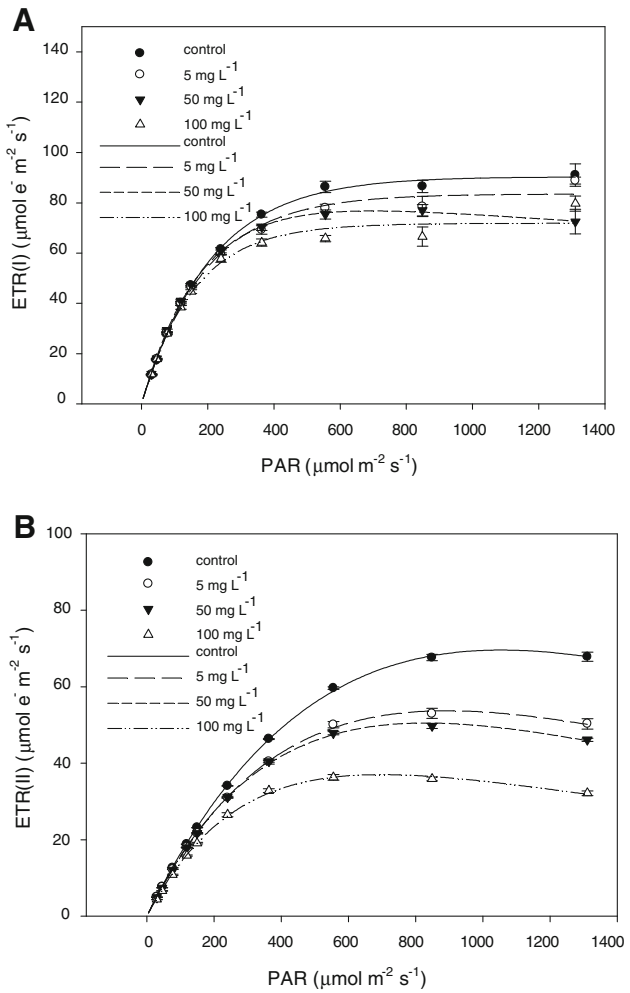

Fig. 3 The rapid light curves (RLCs) of ETR(I) (**a**) and ETR(II) (**b**) after exposure to various concentrations of Sb(V) for 72 h. Data were detected through the light response reaction, where PAR was increasing gradually as 30, 46, 77, 119, 150, 240, 363, 555, 849, and 1,311 (μmol/m^2/s). Data were presented as mean ± SE ($n = 4$). The fitting curves according to Platt et al. [23] were also shown in the graphs

α and ETR_{max} of the RLCs of ETR(II) were lower than those of ETR(I) under various concentrations of Sb(V) treatments and decreased with increasing Sb(V) concentration. α of the RLCs of ETR(II) were significantly lower at 100 mg/l Sb(V) compared to control ($P < 0.05$, DMRT). I_k and ETR_{max} of the RLCs of ETR(II) decreased significantly with increasing Sb(V) concentration. There were significant differences between each treatment ($P < 0.05$, DMRT).

Rapid light curves of cyclic electron transport rate generally increased with increase of the illumination. CEF from the RLCs of cells treated with Sb(V) were higher than control (Fig. 4). The differences became significant with increasing illumination. CEF of the cells exposed to Sb(V) was significantly higher at light intensity above 849 μmol photons/m^2/s compared to control (Fig. 4).

Discussion

In the present study, toxic effects of Sb(V) on the PSI and PSII activities of *M. aeruginosa* were examined. The quantum yields and electron transport rates of PSI, PSII, and CEF under Sb(V) treatment were analyzed.

Toxicity of Sb to organisms is a growing concern. Some recent studies have improved the knowledge of toxicity of Sb to the growth and photosynthesis of plants or microorganisms. Sb in the growth media could lead to the suppression of leaf and root biomass production [21, 26]. High concentrations of Sb could induce toxic symptoms such as chlorosis and leaf necrosis in sunflower and maize [32]. A few recent studies show that both Sb(III) and Sb(V) are toxic to photosynthetic apparatus of cyanobacteria. 1.0 to 10.0 mg/l Sb(III), in the form of antimony potassium tartrate, inhibits O_2 evolution, and both the donor and the acceptor sides of PSII of *Synechocystis* sp. Exposure to Sb(III) led to inhibition of PSII activities and electron transport from Q_A^- to Q_B/Q_B^-, accumulation of P_{680}^+ and increases in the proportion of $PSII_X$ and $PSII_\beta$ [35]. Comparatively, Sb(V) in the form of potassium pyroantimonate has less toxicity to *M. aeruginosa*. Sb(V) at 50 mg/l or higher concentrations inhibits the electron transport on the donor side of PSII and reduces the density of reaction centers [33]. In the present

Table 2 Descriptive parameters of the light response of ETR(I) and ETR(II)

Sb(V) concentration (mg/l)	Parameters of the light response of PSI			Parameters of the light response of PSII		
	I_k (μmol photons/m^2/s)	α (e^-/photon)	ETR_{max} (μmol e^-/m^2/s)	I_k (μmol photons/m^2/s)	α (e^-/photon)	ETR_{max} (μmol e^-/m^2/s)
0	207.7 ± 10.1[a]	0.438 ± 0.010[b]	90.7 ± 2.8[a]	366.1 ± 8.8[a]	0.199 ± 0.001[a]	72.8 ± 1.3[a]
5	190.6 ± 9.3[a]	0.440 ± 0.011[b]	83.6 ± 2.4[a,b]	273.7 ± 7.8[b]	0.197 ± 0.001[a]	54.0 ± 1.4[b]
50	155.4 ± 9.6[b]	0.494 ± 0.014[a]	76.3 ± 2.8[b,c]	245.6 ± 4.0[c]	0.204 ± 0.002[a]	50.1 ± 0.6[c]
100	158.1 ± 6.8[b]	0.456 ± 0.008[b]	72.0 ± 2.1[c]	187.3 ± 4.1[d]	0.191 ± 0.003[b]	35.8 ± 0.6[d]

Data were derived by fitting the RLCs to the exponential function referring to Platt et al. [23]. The measurements were carried out after exposure to various concentrations of Sb(V) for 72 h

[a, b, c, d] Data were mean ± SE ($n = 4$), and data followed by different letters in the same column are significantly different ($P < 0.05$, DMRT)

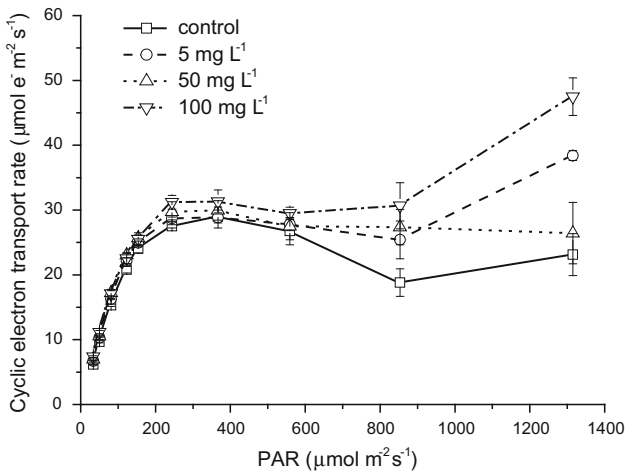

Fig. 4 Cyclic electron transport rate after exposure to various concentrations of Sb(V) for 72 h. Data were detected during the light response reaction, where PAR was increasing gradually as 30, 46, 77, 119, 150, 240, 363, 555, 849, and 1,311 (μmol/m^2/s). Data were presented as mean ± SE ($n = 4$)

study, *Y*(II) decreased significantly with increasing Sb(V) concentration with significant differences between each treatment (Fig. 1; Table 1). *Y*(NO) increased significantly as Sb(V) concentration increased, and *Y*(NO) was significantly higher for cells exposed to Sb(V) compared to control (Table 1). *Y*(NO) is a good indicator of PSII damage, which reflects the fraction of energy that is passively dissipated in the form of heat and fluorescence [9, 31]. The decrease of *Y*(II) and the increase of *Y*(NO) indicate the damage to PSII centers after Sb(V) exposure, which was in accordance with previous study [33].

The quantum yields in PSI showed higher tolerance to Sb(V) than PSII, indicated by the less decrease of *Y*(I) in the whole RLCs than that of PSII (Fig. 1; Table 1). Change of quantum yield distribution between the photosystems and the relation of CEF and LEF could be derived from the change of *Y*(CEF)/*Y*(I), *Y*(II)/*Y*(I), and *Y*(CEF)/*Y*(II) (Fig. 2). Although both *Y*(I) and *Y*(II) decreased after the cells were exposed to various concentrations of Sb(V), the significant decrease of *Y*(II) caused the decrease of the ratio of *Y*(II)/*Y*(I). The decrease of the ratio of *Y*(II)/*Y*(I) with increasing Sb(V) concentration showed imbalanced distribution of quantum yields between the photosystems, suggesting that Sb(V) has more serious inhibition of PSII than PSI. The increase of *Y*(CEF)/*Y*(II) under Sb(V) treatment indicates the activation of CEF and inhibition of LEF. The contribution of *Y*(CEF) to the quantum yield and activity of PSI increased with increasing Sb(V) concentration (Fig. 2).

Some studies test the effects of heavy metals on PSI and suggest that PSI is less sensitive to heavy metals than PSII [2, 27]. Wang et al. [34] investigated the effects of Cr(VI) on the activities of PSI and PSII simultaneously and found that Cr(VI) showed more inhibition of PSII than PSI. The less sensitivity of PSI to heavy metals was also indicated by the less decrease of *Y*(I) and ETR(I) under Sb(V) treatment in the present study.

Y(I) began to show significant decrease when the cells were treated with ≥50 mg/l Sb(V) compared to control, which was associated with the increase of *Y*(ND). *Y*(ND) was the quantum yield of energy dissipation due to donor-side limitations of PSI, and the *Y*(ND) enhanced with the damage to PSII [9]. Huang et al. [10] also suggested that activation of CEF and inhibition of LEF decreased the fraction of PSII electron acceptors that were reduced and then increased the value of *Y*(ND). Activation of CEF and inhibition of LEF, and the increase of *Y*(ND) under Sb(V) treatment were also observed in the present study.

The activation of CEF caused increasing contribution of *Y*(CEF) to *Y*(I) (Fig. 2). Similarly, cyclic electron transport made big contribution to electron transport of PSI when the cells were exposed to Sb(V). It was shown by the increase of cyclic electron transport rate after Sb(V) treatment and the values of ETR(I), especially at high Sb(V) concentration (100 mg/l) and high illumination (above 555 μmol photons/m^2/s) (Figs. 3, 4). The enhancement of the contribution of CEF to the quantum yield of PSI was important for the less sensitivity of PSI to Sb(V) treatment, similar to

the results of *M. aeruginosa* exposed to Cr(VI) stress [34]. The stimulation of CEF led to less change of descriptive parameters of the light response of ETR(I) than ETR(II), such as the photon-capturing efficiency (α) and the light saturation coefficient (I_k). Sb(V) also caused less decrease of ETR_{max} of PSI than that of PSII. These results confirmed that the stimulation of CEF was essential for the less sensitivity and the protection of PSI under stress of Sb(V) and other stresses [6, 9].

Cyclic electron flow has essential functions in both photoprotection and photosynthesis [18, 25]. CEF is very sensitive to photosystem interference induced by chemicals and that the PGR5 pathway is very critical for regulation [24]. CET can balance the ATP/NADPH production ratio to protect photosystems under environmental stress by inducing non-photochemical quenching (qN) to dissipate excessive absorbed light energy [10, 11, 25]. In the present study, the cells treated with Sb(V) could still maintain their *Y*(NPQ) (Table 1), which might benefit from the activation of CEF.

In the present study, Sb was applied at higher concentrations than those found in normal surface water, but comparable to Sb levels in wastewater and surface water near the mining area [7]. The concentrations of Sb in wastewater, river waters, and polluted well water near the Xikuangshan Sb mine in Hunan Province of China are 1.33–21.79, 0.063–0.037, and 24.02–42.03 mg/l, respectively [7]. Sb in topsoil near this mine is up to 5,045 mg/kg [8]. In the present study, treatments with Sb at concentration up to 100 mg/l can be used to provide the data on the acute toxicity of Sb to the activities of two photosystems of *M. aeruginosa*. The activities of two photosystems and the physiological characteristics of CEF were detected simultaneously. The lowest Sb (V) concentration (5 mg/l) used in the experiment significantly inhibited PSII activity, but had no significant effects on PSI activity. At higher concentrations of Sb(V) in the present study, the quantum yield and electron transport of PSI were less affected than those of PSII. These results indicated that PSII was a sensitive site to heavy metals as suggested by previous studies [1, 33], while PSI was less sensitive. Sb(V) led to imbalanced distribution of quantum yields between two photosystems and more serious inhibition of photochemistry quantum yield of PSII than PSI. The results also showed the activation of CEF and inhibition of LEF under Sb(V) treatment. The enhancement of the contribution of CEF to the quantum yield of PSI was important for the less sensitivity of PSI to Sb(V) treatment. The stimulation of CEF increased the tolerance of PSI to Sb(V).

Acknowledgments This work was supported by the National Natural Science Foundation of China (U1120302).

References

1. Appenroth KJ, Stöckel J, Srivastava A, Strasser RJ (2001) Multiple effects of chromate on the photosynthetic apparatus of *Spirodela polyrhiza* as probed by OJIP chlorophyll *a* fluorescence measurements. Environ Pollut 115:49–64
2. Atal N, Saradhi PP, Mohanty P (1991) Inhibition of the chloroplast photochemical reactions by treatment of wheat seedlings with low concentrations of cadmium: analysis of electron transport activities and changes in fluorescence yield. Plant Cell Physiol 32:943–951
3. Bustamante J, Dock L, Vahter M, Fowler B, Orrenius S (1997) The semiconductor elements arsenic and indium induce apoptosis in rat thymocytes. Toxicology 118:129–136
4. Coopman RE, Fuentes-Neira FP, Briceño VF, Cabrera HM, Corcuera LJ, Bravo LA (2010) Light energy partitioning in photosystems I and II during development of *Nothofagus nitida* growing under different light environments in the Chilean evergreen temperate rain forest. Trees Struct Funct 24:247–259
5. Deng C, Zhang D, Pan X, Chang F, Wang S (2013) Toxic effects of mercury on PSI and PSII activities, membrane potential and transthylakoid proton gradient in *Microsorium pteropus*. J Photochem Photobiol B: Biol 127:1–7
6. Gao S, Wang G (2012) The enhancement of cyclic electron flow around photosystem I improves the recovery of severely desiccated *Porphyra yezoensis* (Bangiales, Rhodophyta). J Exp Bot 63:4349–4358
7. He M, Yang J (1999) Effects of different forms of antimony on rice during the period of germination and growth and antimony concentration in rice tissue. Sci Total Environ 243–244:149–155
8. He MC, Ji HB, Zhao CY, Xie J, Wu XM, Li ZF (2002) Preliminary studies of heavy metal pollution in soil and plant near antimony mine area. J Beijing Normal University (Nat Sci) 38:417–420
9. Huang W, Zhang S-B, Cao K-F (2010) Stimulation of cyclic electron flow during recovery after chilling-induced photoinhibition of PSII. Plant Cell Physiol 51:1922–1928
10. Huang W, Yang SJ, Zhang SB, Zhang JL, Cao KF (2012) Cyclic electron flow plays an important role in photoprotection for the resurrection plant *Paraboea rufescens* under drought stress. Planta 235:819–828
11. Johnson GN (2011) Physiology of PSI cyclic electron transport in higher plants. Biochim Biophys Acta 1807:384–389
12. Jones RD (1994) Survey of antimony workers: mortality 1961-1992. Occup Environ Med 51:772–776
13. Klughammer C, Schreiber U (1994) An improved method, using saturating light pulses, for the determination of photosystem I quantum yield via $P700^+$-absorbance changes at 830 nm. Planta 192:261–268
14. Klughammer C, Schreiber U (2008) Complementary PS II quantum yields calculated from simple fluorescence parameters measured by PAM fluorometry and the Saturation Pulse method. PAM Appl Notes 1:27–35
15. Klughammer C, Schreiber U (2008) Saturation Pulse method for assessment of energy conversion in PS I. PAM Appl Notes 1:11–14
16. Kramer DM, Johnson G, Kiirats O, Edwards GE (2004) New fluorescence parameters for the determination of Q_A redox state and excitation energy fluxes. Photosynth Res 79:209–218
17. Kühl M, Glud RN, Borum J, Roberts R, Rysgaard S (2001) Photosynthetic performance of surface-associated algae below sea ice as measured with a pulse-amplitude-modulated (PAM) fluorometer and O_2 microsensors. Mar Ecol Prog Ser 223:1–14

18. Munekage Y, Hashimoto M, Miyake C, Tomizawa KI, Endo T, Tasaka M, Shikanai T (2004) Cyclic electron flow around photosystem I is essential for photosynthesis. Nature 429:579–582
19. Nam S-H, Yang C-Y, An Y-J (2009) Effects of antimony on aquatic organisms (Larva and embryo of *Oryzias latipes*, *Moina macrocopa, Simocephalus mixtus*, and *Pseudokirchneriella subcapitata*). Chemosphere 75:889–893
20. Nitschke U, Connan S, Stengel DB (2012) Chlorophyll *a* fluorescence responses of temperate Phaeophyceae under submersion and emersion regimes: a comparison of rapid and steady-state light curves. Photosynth Res 114:29–42
21. Pan XL, Zhang D, Chen X, Bao AM, Li LH (2011) Antimony accumulation, growth performance, antioxidant defense system and photosynthesis of *Zea mays* in response to antimony pollution in soil. Water Air Soil Pollut 215:517–523
22. Pfündel E, Klughammer C, Schreiber U (2008) Monitoring the effects of reduced PS II antenna size on quantum yields of photosystems I and II using the Dual-PAM-100 measuring system. PAM Appl Notes 1:21–24
23. Platt T, Gallegos CL, Harrison WG (1980) Photoinhibition of photosynthesis in natural assemblages of marine phytoplankton. J Mar Res 38:687–701
24. Qian H, Tsuji T, Endo T, Sato F (2014) PGR5 and NDH pathways in photosynthetic cyclic electron transfer respond differently to sublethal treatment with photosystem-interfering Herbicides. J Agric Food Chem 62:4083–4089
25. Shikanai T (2007) Cyclic electron transport around photosystem I: genetic approaches. Annu Rev Plant Biol 58:199–217
26. Shtangeeva I, Bali R, Harris A (2011) Bioavailability and toxicity of antimony. J Geochem Explor 110:40–45
27. Siedlecka A, Krupa Z (1996) Interaction between cadmium and iron and its effects on photosynthetic capacity of primary leaves of *Phaseolus vulgaris*. Plant Physiol Biochem 34:833–841
28. Smichowski P (2008) Antimony in the environment as a global pollutant: a review on analytical method ologies for its determination in atmospheric aerosols. Talanta 75:2–14
29. Stanier RY, Kunisawa R, Mandel M, Cohen-Bazire G (1971) Purification and properties of unicellular blue-green algae (order *Chroococcales*). Bacteriol Rev 35:171–205
30. Sun FH, Wu FC, Liao HQ, Xing BS (2011) Biosorption of antimony(V) by freshwater cyanobacteria Microcystis biomass: chemical modification and biosorption mechanisms. Chem Eng J 171:1082–1090
31. Suzuki K, Ohmori Y, Ratel E (2011) High root temperature blocks both linear and cyclic electron transport in the dark during chilling of the leaves of rice seedlings. Plant Cell Physiol 52:1697–1707
32. Tschan M, Robinson B, Johnson CA, Bürgi A, Schulin R (2010) Antimony uptake and toxicity in sunflower and maize growing in Sb^{III} and Sb^{V} contaminated soil. Plant Soil 334:235–245
33. Wang S, Pan X (2012) Effects of Sb(V) on growth and chlorophyll fluorescence of *Microcystis aeruginosa* (FACHB-905). Curr Microbiol 65:733–741
34. Wang S, Chen F, Mu S, Zhang D, Pan X, Lee D-J (2013) Simultaneous analysis of photosystem responses of *Microcystis aeruginoga* under chromium stress. Ecotoxicol Environ Saf 88:163–168
35. Zhang DY, Pan XL, Mu GJ, Wang JL (2010) Toxic effects of antimony on photosystem II of *Synechocystis* sp. as probed by in vivo chlorophyll fluorescence. J Appl Phycol 22:479–488
36. Zhou W, Juneau P, Qiu B (2006) Growth and photosynthetic responses of the bloom-forming cyanobacterium *Microcystis aeruginosa* to elevated levels of cadmium. Chemosphere 65:1738–1746